15 Sep 2022

Effects of Radiation Reabsorption on the Laminar Flame Speed and NO Emission during Aviation Kerosene Combustion at Elevated Pressures

Shu Zheng

Hao Liu

Qing Li

Jiajian Zhu

et. al. For a complete list of authors, see https://scholarsmine.mst.edu/mec_aereng_facwork/4927

Recommended Citation

S. Zheng et al., "Effects of Radiation Reabsorption on the Laminar Flame Speed and NO Emission during Aviation Kerosene Combustion at Elevated Pressures," *Fuel*, vol. 324, article no. 124545, Elsevier, Sep 2022.
The definitive version is available at https://doi.org/10.1016/j.fuel.2022.124545

Fuel 324 (2022) 124545

Contents lists available at ScienceDirect

Fuel

journal homepage: www.elsevier.com/locate/fuel

Full Length Article

Effects of radiation reabsorption on the laminar flame speed and NO emission during aviation kerosene combustion at elevated pressures

Shu Zheng [a,b], Hao Liu [b], Qing Li [a,*], Jiajian Zhu [a], Mingbo Sun [a], Bo Zhou [c], Ran Sui [d], Qiang Lu [b,*]

[a] College of Aerospace Science and Engineering, National University of Defense Technology, Hunan 410073, China
[b] National Engineering Research Center of New Energy Power Generation, North China Electric Power University, Beijing 102206, China
[c] Department of Mechanics and Aerospace Engineering, Southern University of Science and Technology, Shenzhen 518055, China
[d] Department of Mechanical and Aerospace Engineering, Missouri University of Science and Technology, Rolla, MO 65409, United States

ARTICLE INFO

Keywords:
Aviation kerosene
Radiation reabsorption
Vitiated air
Laminar flame speed
NO emission
Statistical narrow-band model (SNB)

ABSTRACT

Increasing attention has been paid on combustion stability and pollution emission of aviation kerosene due to the emerging interests on supersonic combustion scramjets. Whereas, the vitiation component H_2O introduced by hydrogen-fueled heaters in high-enthalpy vitiated air during ground experiments has a considerable influence on kerosene combustion, especially through its radiation effect, which needs to be further investigated. In this paper, the radiation reabsorption effects on laminar flame speeds and NO emissions during RP-3/H_2O/O_2/N_2 combustion was assessed numerically over a wide range of equivalence ratio and pressure (ϕ = 0.7–1.4 and P = 1–15 atm) using detailed chemical and radiation models. The surrogate model of RP-3 consisted of vol. 25% 1,3,5-trimethylbenzene (C_9H_{12}), 46.31% *n*-decane ($C_{10}H_{22}$) and 28.69% iso-dodecane ($IC_{12}H_{26}$), while the vitiated air had 12% H_2O. It was revealed that the radiation reabsorption of H_2O in the vitiated air had significant impact on the accurate simulation of laminar flame speeds. As equivalence ratios varied, the role of radiation reabsorption on laminar flame speeds was most pronounced at ϕ = 0.7. As the key radical, the generation of H through the reversed step of $CH_2OH + H = CH_3 + OH$ was chemically inhibited due to radiation. The radiation reabsorption effect on flame speeds was strengthened with rising pressures, with the reaction $H + O_2 = O + OH$ dominant at the pressure range 1–10 atm. In contrast, a slight increase in the impact on laminar flame speeds between 10 and 15 atm was controlled by direct radiative effect. Finally, for NO emission, the reduction of downstream temperature caused by radiative heat loss and the increment of radical concentrations induced by preheating determined radiation reabsorption effects on NO generation.

1. Introduction

Supersonic combustion scramjets, which can produce 4 times as much thrust as rockets with the same mass of propellant due to their super dynamic characteristics, are of increasing interest to both civil and defense applications [1]. As the main fuel of aero-engines including scramjets, the combustion performance of aviation kerosene directly affects the stability and economy of aircrafts [2]. Laminar flame speed is an indicator of basic combustion characteristics of aviation kerosene, which can be also used to verify chemical reaction mechanisms and as the basis of research on other combustion problems. Hence, accurate calculation of kerosene's laminar flame speed is an important reference index for aero-engine designs [3]. On the other hand, along with the increasingly strict environmental policies, it is also of vital importance to investigate the pollutant emissions of aviation kerosene [4].

Sufficient ground experiment is the premise of scramjet flight design and the high-enthalpy experimental gas is a key factor to simulate hypersonic states. However, hydrogen-fueled heaters, the widely used combustion heating method at present, introduce vitiation component H_2O that affects kerosene combustion and engine operation [5]. Sun et al. [6] investigated the auto-ignition of RP-3 kerosene under air and vitiated air conditions. The ignition delay times (IDTs) data of RP-3 kerosene with various H_2O contents (0–20% by mole) in vitiated air were collected and the thermal and chemical effects of H_2O vitiation on the kerosene combustion were explored. They found that the linear pressure dependence for IDTs of RP-3 was inhibited by H_2O vitiation, the

* Corresponding authors.
E-mail addresses: qing.li@nudt.edu.cn (Q. Li), qianglu@mail.ustc.edu.cn (Q. Lu).

https://doi.org/10.1016/j.fuel.2022.124545
Received 31 March 2022; Received in revised form 25 April 2022; Accepted 6 May 2022
Available online 12 May 2022

thermodynamic properties of H_2O dominated at low pressures and the chemical effect was more significant at high pressures. Then, the experimental investigation on flame stabilization of kerosene combustion was conducted by Shi [7] in a scramjet combustor, with the molar compositions of vitiated air 12% H_2O, 21% O_2 and 67% N_2. Results showed that successful ignition and stable combustion of kerosene was only observed when pilot hydrogen, a component of kerosene, was within certain equivalence ratios. Besides, Chang et al. [8] examined the effects of H_2O on NO emission in *n*-decane/air flames, which is an important component of aviation kerosene, and reported the NO formation pathway was changed at different equivalence ratios and pressures due to the H_2O effect. Hence, the impact of vitiation component H_2O on the laminar flame speed and NO emission for kerosene combustion should be taken into account.

Moreover, as a strong radiative species, the radiation effect of H_2O on combustion processes cannot be ignored. Ju et al. [9] first identified the radiative heat loss and reabsorption effects of $CH_4/O_2/N_2/CO_2$ mixtures via the discrepancies in the absorption spectra of H_2O and CO_2. Substantially higher flame speed and wider flammability limits were observed when radiation effects were considered. Subsequently, Yoshinaga et al. [10] conducted a numerical study on polypropylene combustion concerned with the radiation effects of H_2O and CO_2. Results verified that the gas radiation of H_2O and CO_2, two strong radiative species, had a great influence on polypropylene combustion, which reflected that the statistical narrow-band model (SNB) was more accurate than the optically thin model (OTM) under high temperature conditions because SNB considered radiation reabsorption on the basis of OTM. Furthermore, Sohn et al. [11] quantitatively evaluated the radiation effect on flame speed in spherical $CO/CO_2/H_2O$-diluted CH_4/air and H_2/air flames, and indicated that the underestimation of flame speed caused by radiative heat loss could be up to 17%. Likewise, radiation effect on NO emission was assessed by Wang et al. [12] for CH_4/air counterflow flames with CO_2 dilution, where a slight overestimation on the maximum flame temperature (by 52 K and about 3.5%) resulted from radiation reabsorption caused a significant error in the prediction of NO mole fraction (by 28%). Even though the radiation effect on combustion parameters has been proven to be significant, the radiation reabsorption effects on aviation kerosene combustion have not been studied.

The radiation reabsorption effects of H_2O in vitiated air on the laminar flame speeds and NO emission during kerosene combustion were revealed in this paper, with the equivalence ratios ranging from 0.7 to 1.4 and pressures up to 15 atm. The radiation reabsorption effects on laminar flame speeds and NO emission were quantified by comparisons with adiabatic model under different conditions (equivalence ratios and pressures). Then, the thermal effect and chemical effect of radiation reabsorption were analyzed via sensitivity analyses and reaction pathway analyses. Eventually, the influencing mechanism of radiation reabsorption on laminar flame speeds and NO emission under different equivalence ratios and pressures were discussed.

2. Computational details

As a conventional petroleum-derived jet fuel, China NO. 3 aviation kerosene (RP-3) is easy to obtain and produce, with the advantages of inexpensive and can be long-term storage, which is the most widely applied fuel of aero-engines in China [13]. RP-3 is mainly composed of C_{10}-C_{16} hydrocarbons, including alkanes, cycloalkanes and aromatic hydrocarbons, etc., among which the alkanes have the largest proportion, followed by aromatic hydrocarbons and cycloalkanes [14]. Because of the complex compositions of real aviation kerosene, numerical studies are generally performed using surrogate models composed of several important components, which can reproduce the physical and chemical characteristics of the actual fuel. Liu's surrogate model [15] captured the essential properties RP-3 kerosene, including octane number, lower heating value, molecular weight and C/H ratio, and was hence adopted in this study. The surrogate model consists of three components: 1,3,5-trimethylbenzene (C_9H_{12}), *n*-decane ($C_{10}H_{22}$) and iso-dodecane ($iC_{12}H_{26}$) with respective mole fractions of 25%, 46.31% and 28.69%.

One-dimensional planar flames were simulated using the PREMIX code [16] of CHEMKIN, which computes the temperature and species profiles in premixed laminar flames. A detailed reaction mechanism (90 species and 449 reactions) was adopted in this work, combining Liu's kinetic model [15] and the NOMecha2.0 model [17], the detailed contents of the final mechanism applied were attached in the Supplementary materials. To verify this kinetic model, the laminar flame speeds of RP-3 kerosene/air flame were calculated and compared with the experimental results measured though a constant volume combustion chamber [3] (shown in Fig. 1). Results indicated that this mechanism was reliable to reproduce the laminar flame speeds of RP-3 flames, even under high pressures. Considering the uncertainties in the experiment and the influence of surrogate model and linear extrapolation of stretch rate, the errors between the experiment and simulation were considered acceptable. Moreover, the absolute relative errors between the final mechanism (with the addition of NO sub-model) and the original kinetic model in predicting the laminar flame speed of RP-3 mixtures were less than 3%. Therefore, we considered that the introduction of NO sub-model does not affect the accuracy of Liu's model, which have been extensively validated [15].

To fully account for the radiation effects, the radiation parameters of H_2O, a strong radiating species, were calculated based on the HITRAN 2016 database and were included in the statistical narrow-band model (SNB) [18]. The detailed calculation formula and accuracy verification of SNB model can be referred to our previous studies [19–22]. As a demonstration, Fig. 2 shows the structure (including profiles of flame temperatures and major radicals) of an RP-3/$H_2O/O_2/N_2$ flame (ϕ = 1.0, $H_2O/O_2/N_2$ = 12%/21%/67%) calculated by the adiabatic model (ADI) and SNB. Compared to the conventional model ADI that does not consider any radiation effects, the SNB model takes into account both the external radiative heat loss and internal radiative heat transfer [23]. Thus, the temperature of the unburned mixture was elevated by the thermal radiation transmitted from downstream (by ~30 K, see the left insert in the temperature subfigure) and temperature of the burned zone decreased due to radiative heat loss by more than 100 K at X > 20 cm. Meanwhile, the profiles of radicals were also affected by radiation reabsorption. The peak concentrations of radicals obtained by SNB were all higher than those by ADI because of the temperature sensitivity of

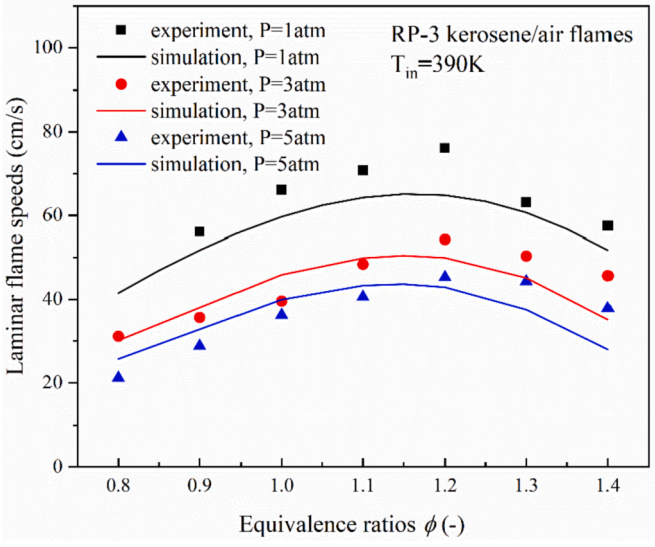

Fig. 1. Comparisons between the experimental data and the simulation results of laminar flame speed for RP-3/air mixtures. (ϕ = 0.8–1.4, P = 1, 3, 5 atm, T_{in} = 390 K). Experimental data from Ma et al. [3].

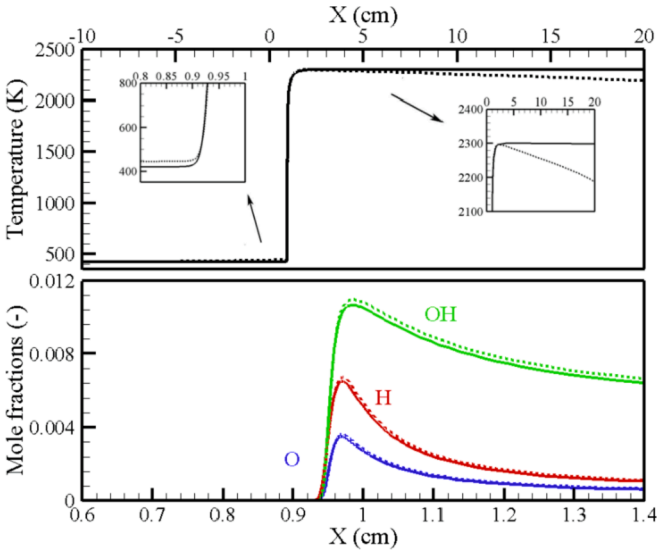

Fig. 2. Flame structures calculated by ADI and SNB models for an RP-3/H_2O/O_2/N_2 flame (ϕ = 1.0, P = 1 atm, $H_2O/O_2/N_2$ = 12%/21%/67%). Solids lines are ADI results and dashed lines SNB results.

chain initiation reactions [20], which also resulted in the increment of laminar flame speeds that will be discussed in the following sections.

3. Results and discussion

3.1. Effects on laminar flame speeds

3.1.1. At various equivalence ratios

The laminar flame speeds at atmospheric pressure with various equivalence ratios ϕ for RP-3/H_2O/O_2/N_2 flames are depicted in Fig. 3. The inlet temperature was 420 K and equivalence ratios ranged from 0.7 to 1.4. Because the high-enthalpy vitiated air used in ground experiment was provided by the combustion of hydrogen, oxygen, and air in a heater, the H_2O was introduced and molar composition of vitiated air was 21% O_2, 12% H_2O and 67% N_2, according to the practical conditions typically adopted in ground experiments [2,24]. It can be seen that the computed laminar flame speeds, both calculated by ADI and SNB, first increased and then decreased with rising equivalence ratios ϕ, with the peak values (67.30 cm/s for ADI and 70.03 cm/s for SNB) occurred at ϕ = 1.15. In the whole range of the investigated equivalence ratios, the laminar flame speeds calculated by SNB were consistently higher than ADI. Their relative differences, quantified as $(S_{L,SNB}-S_{L,ADI})/S_{L,ADI}$, decreased from 12.60% to 4.04% at ϕ = 0.7–1.2 and subsequently increased to 5.69% when ϕ = 1.4.

As reported in our previous studies [19–21], the roles of radiation reabsorption were determined by physical factors firstly, namely optical thickness and absorption coefficient. As manifested in Fig. 4, the (blocking) optical thickness defined by the system dimension and Plank mean absorption length [19] first decreased and then increased as the equivalence ratio increased. As for the factor that affected radiation absorption, the absorption coefficient, which was proportional to the mole fraction of the strongly radiating medium H_2O in the upstream, exhibited a decreasing trend. Combining these two aspects, the direct radiative effect on laminar flame speeds should increase first and then decrease (mainly controlled by optical thickness, because the X_{H2O} changed slightly at various equivalence ratios), which was inconsistent with the relative difference of laminar flame speed shown in Fig. 3. Therefore, the chemical effect of radiation reabsorption should be the main factor affecting the laminar flame speed at various equivalence ratios for RP-3/H_2O/O_2/N_2 flames.

To explore the mechanism that radiation reabsorption chemically affected the laminar flame speeds, sensitivity analyses for laminar flame speeds were performed at various equivalence ratios and the reactions with top sensitivity coefficients are listed in Fig. 5. The most positively sensitive reaction for laminar flame speeds was H + O_2 = O + OH among all equivalence ratios. For negatively sensitive reactions, H + OH + M = H_2O + M was dominant in fuel-lean combustion, while HCO + H = CO + H_2 and C_3H_7 = C_3H_6 + H were also important at the two investigated fuel-rich equivalence ratios. Among the three fuel components, only the first step H-abstraction reaction of C_9H_{12} (C_9H_{12} (+M) = H + $C_8H_9CH_2$ (+M)) had a significant impact on the laminar flame speed, since the other fuels preferred to react with OH radical (via $iC_{12}H_{26}$ + OH = $iC_{12}H_{25}$ + H_2O and $C_{10}H_{22}$ + OH = $C_{10}H_{21}$ + H_2O). In addition, the sensitivity coefficient of reaction CO + OH = CO_2 + H varied significantly at various equivalence ratios because more H radicals were converted into OH through H + O_2 = O + OH at oxygen-rich conditions. Based on the most sensitive reactions affecting the laminar flame speed as mentioned above (H + O_2 = O + OH, HCO + H = CO + H_2, C_3H_7 = C_3H_6 + H), it can be concluded that the H radicals played a crucial role in determining laminar flame speeds for RP-3/H_2O/O_2/N_2 flames. This was also reflected by the relative difference of peak concentration of H radicals between ADI and SNB at various equivalence ratios shown in Fig. 6, which is in accordance with the relative difference of laminar flame speed shown in Fig. 3.

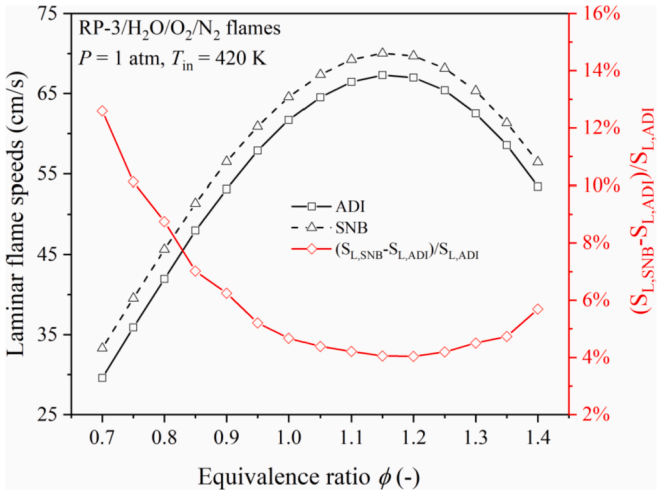

Fig. 3. Laminar flame speeds at various equivalence ratios for RP-3/H_2O/O_2/N_2 mixtures (P = 1 atm, T_{in} = 420 K, $H_2O/O_2/N_2$ = 12%/21%/67%).

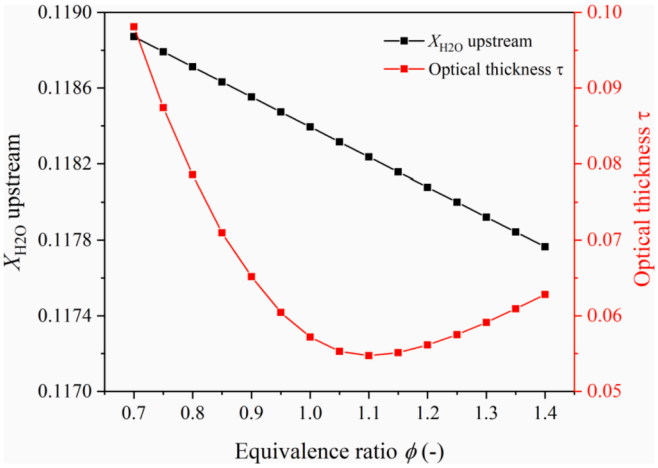

Fig. 4. Optical thickness and mole fraction of H_2O (a factor proportional to absorption coefficient) at various equivalence ratios for RP-3/H_2O/O_2/N_2 mixtures (P = 1 atm, T_{in} = 420 K, $H_2O/O_2/N_2$ = 12%/21%/67%).

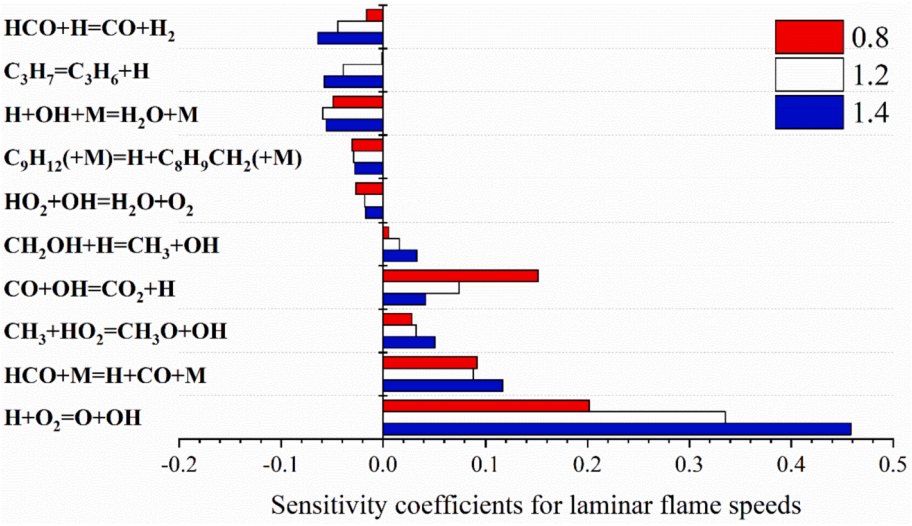

Fig. 5. Sensitivity analysis of laminar flame speeds at three equivalence ratios for RP-3/$H_2O/O_2/N_2$ mixtures (P = 1 atm, T_{in} = 420 K, $H_2O/O_2/N_2$ = 12%/21%/67%).

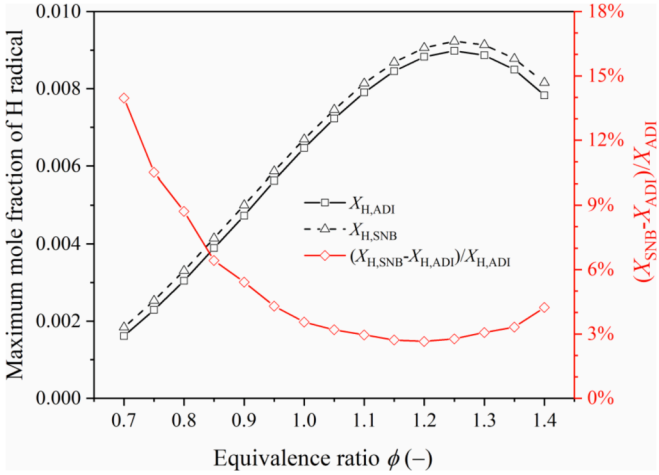

Fig. 6. Peak concentration of H radicals at various equivalence ratios for RP-3/$H_2O/O_2/N_2$ mixtures (P = 1 atm, T_{in} = 420 K, $H_2O/O_2/N_2$ = 12%/21%/67%).

Next, to gain a better insight, sensitivity analysis and rate-of-production (ROP) analysis were conducted for H radicals at various equivalence ratios for RP-3/$H_2O/O_2/N_2$ mixtures. As shown in Fig. 7a, reaction H + O_2 = O + OH was the biggest consumption step of H radicals at all the three simulated equivalence ratios. Among the positive-ROP reactions, CO + OH = CO_2 + H had the highest ROP coefficients when ϕ was 0.8 and 1.2, while O + H_2 = H + OH became strongest when ϕ was further increased to 1.4. Interestingly, these reactions were not among the most sensitive reactions for H radicals as shown in Fig. 7b. The most negatively-sensitive reaction was H + OH + M = H_2O + M and the most positively-sensitive reaction was CH_2OH + H = CH_3 + OH over all the investigated equivalence ratios, which were both among the important ROP reactions in Fig. 7a. It is worthwhile mentioning that CH_2OH + H = CH_3 + OH was reversed because of the abundant CH_3 radicals in the RP-3/$H_2O/O_2/N_2$ flames; the sensitivity coefficient for H radicals of this reaction was positive indicating it facilitated the production of H radicals through its reverse reaction. For the main formation pathway of CH_3 radicals, the main compounds of RP-3 kerosene, $C_{10}H_{22}$ and $iC_{12}H_{26}$, were first dehydrogenated to form $C_{10}H_{21}$ and $iC_{12}H_{25}$, and then decomposed via reactions $C_{10}H_{21}$ = $2C_3H_6$ + C_2H_5 + C_2H_4 and $iC_{12}H_{25}$ = $2C_3H_6$ + C_2H_5 + $2C_2H_4$ to produce large amounts of C_3H_6 and C_2H_4. Subsequently, the CH_3 radicals were generated, mainly by decomposition of C_3H_6 (via C_3H_6 = C_2H3 + CH_3) and reaction of C_2H_4 with OH (C_2H_4 + OH = CH_2O + CH_3). Consequently, the following discussion will be focused on the relative difference of ROP values for reverse reaction of CH_2OH + H = CH_3 + OH when the inlet temperature was preheated due to radiation reabsorption.

Fig. 7 shows the ROP values of reaction CH_2OH + H = CH_3 + OH and its relative difference with inlet two temperatures T_{in} = 420 K and 450 K. When the inlet temperature was elevated, the generation of H radicals by reversed CH_2OH + H = CH_3 + OH was inhibited. The inhibition was strengthened at ϕ = 0.7–1.2 and weakened at ϕ = 1.2–1.4, so that the relative difference of maximum mole fraction for H radicals exhibited a non-monotonic behavior. Moreover, since this reaction possessed positive sensitivity coefficients for laminar flame speeds in Fig. 5, the increasing inhibition on CH_2OH + H = CH_3 + OH depressed its promotion of laminar flame speeds, thus the relative differences of laminar flame speed decreased at ϕ = 0.7–1.2. In contrast, the relative differences increased at ϕ = 1.2–1.4 resulting from the waning inhibition.

3.1.2. *At various pressures*

The impact of radiation reabsorption on laminar flame speed at different pressures is subsequently illustrated in this section. Fig. 8 shows computed laminar flame speeds at various pressures by ADI and SNB and their relative difference caused by radiation reabsorption. As pressure increased, the laminar flame obtained via ADI and SNB both decreased while the radiation reabsorption effect progressively aggravated from 4.67% at 1 atm to 12.41% at 15 atm.

Similar to the previous section, the direct radiative effect on laminar flame speed was examined primarily. Since the absorption coefficient was also proportional to pressure in addition to mole fraction, it is expressed as $X_{H2O}P$ in Fig. 10. Although both optical thickness and $X_{H2O}P$ increased with increasing pressures, $X_{H2O}P$ at the upstream increased more than the optical thickness. This caused the relative difference that laminar flame speed (between SNB and ADI results) slightly increased with rising pressure, as the linear increment at P = 10–15 atm shown in Fig. 9. Whereas the radiation reabsorption effect on laminar flame speed at P = 1–10 atm showed a non-linear tendency, indicating that the chemical effect cannot be ignored at this stage.

Fig. 10 shows the important reactions controlling laminar flame speed at three pressures, 1, 5 and 10 atm. Same as those at various equivalence ratios under atmospheric pressure in Fig. 5, reaction H + O_2 = O + OH had the largest positive sensitivity coefficient among the examined pressures. For negative sensitive reactions, H + OH + M =

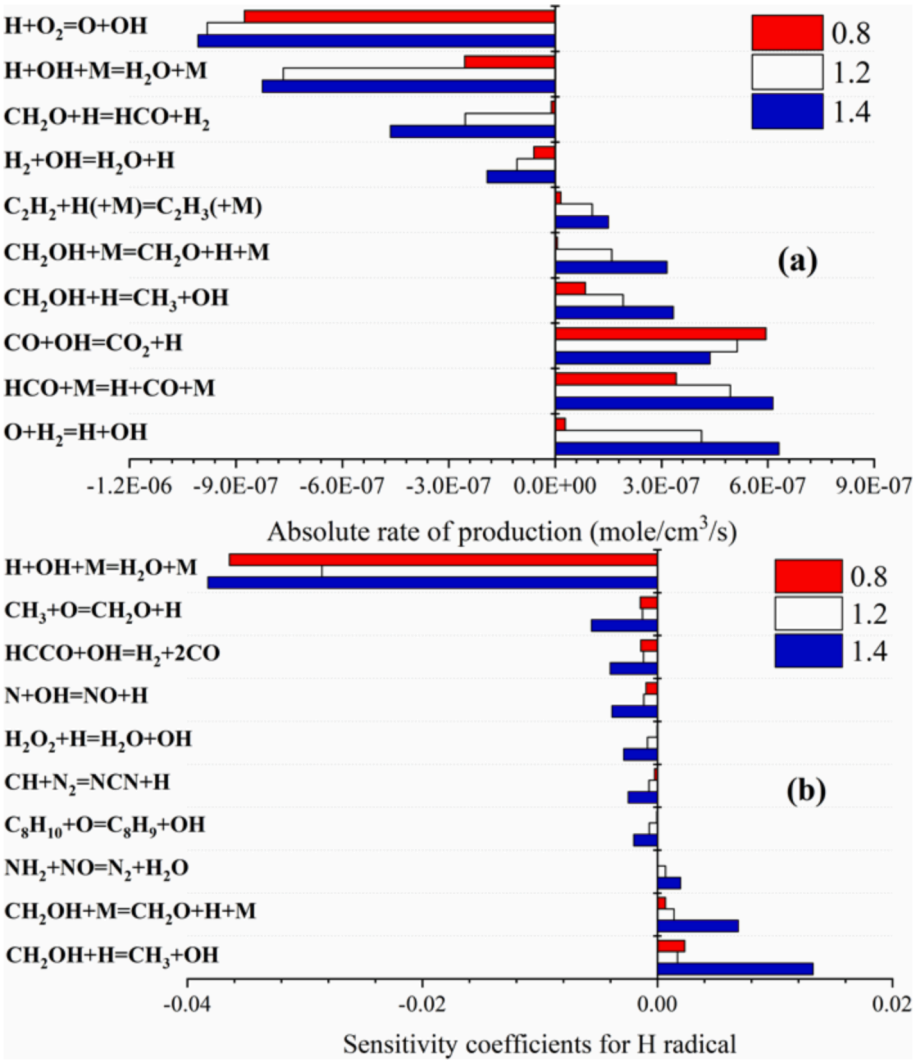

Fig. 7. ROP (a) and sensitivity (b) analyses for H radicals at three equivalence ratios for RP-3/$H_2O/O_2/N_2$ mixtures (P = 1 atm, T_{in} = 420 K, $H_2O/O_2/N_2$ = 12%/21%/67%).

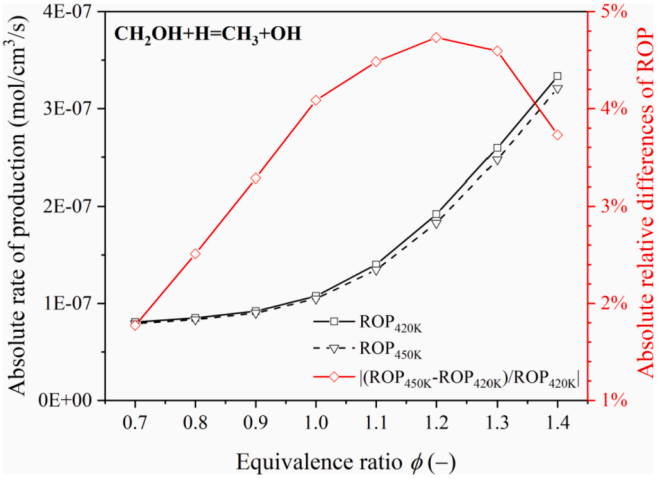

Fig. 8. ROP values for reaction $CH_2OH + H = CH_3 + OH$ with two different inlet temperatures for RP-3/$H_2O/O_2/N_2$ mixtures (P = 1 atm, T_{in} = 420 K and 450 K, $H_2O/O_2/N_2$ = 12%/21%/67%).

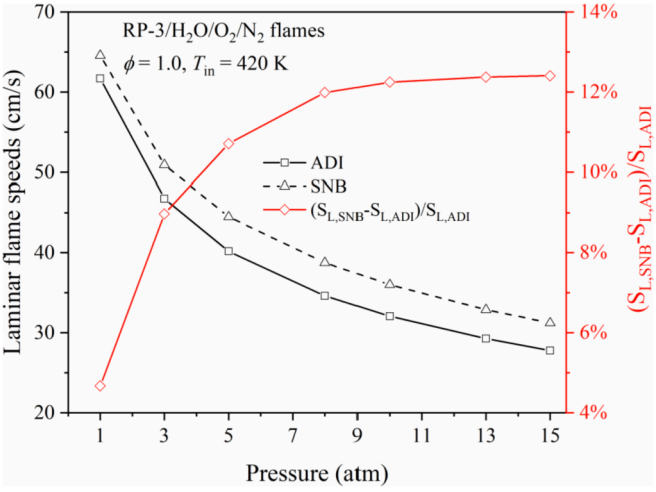

Fig. 9. Laminar flame speeds at various pressures for RP-3/$H_2O/O_2/N_2$ mixtures (ϕ = 1.0, T_{in} = 420 K, $H_2O/O_2/N_2$ = 12%/21%/67%).

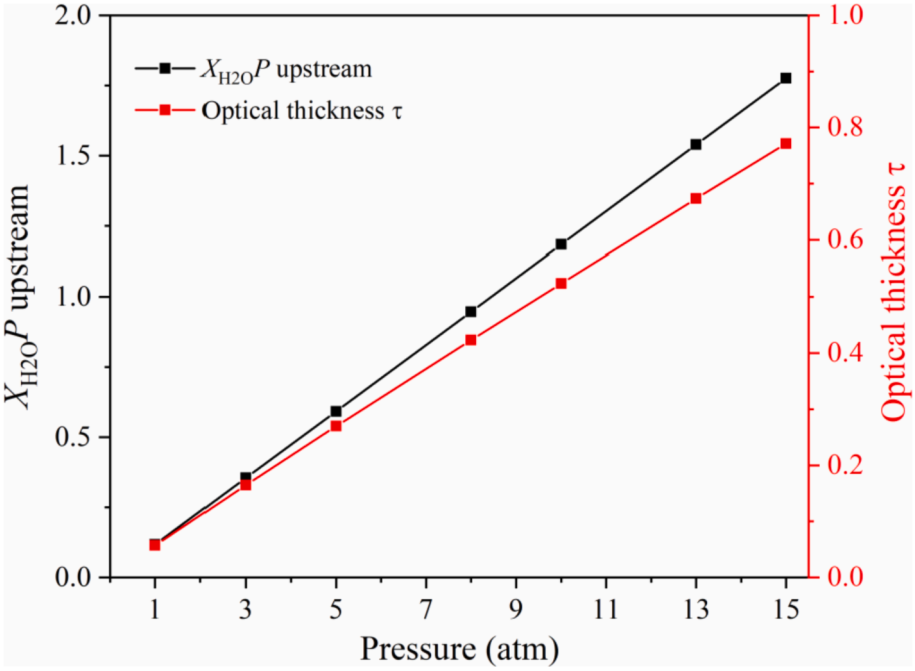

Fig. 10. Optical thickness and absorption coefficient at various pressures for RP-3/$H_2O/O_2/N_2$ mixtures (ϕ = 1.0, T_{in} = 420 K, $H_2O/O_2/N_2$ = 12%/21%/67%).

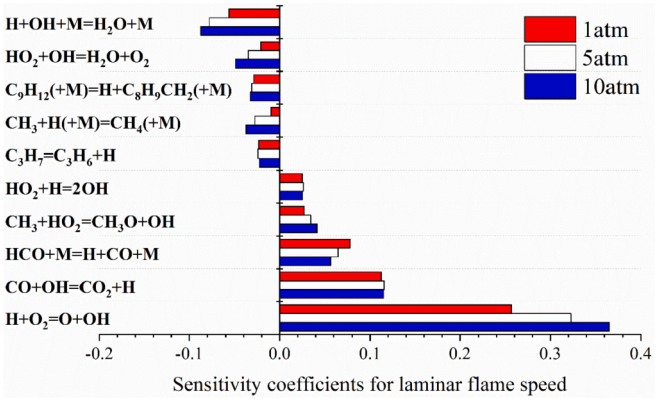

Fig. 11. Sensitivity analysis of laminar flame speed at three pressures for RP-3/$H_2O/O_2/N_2$ mixtures (ϕ = 1.0, T_{in} = 420 K, $H_2O/O_2/N_2$ = 12%/21%/67%).

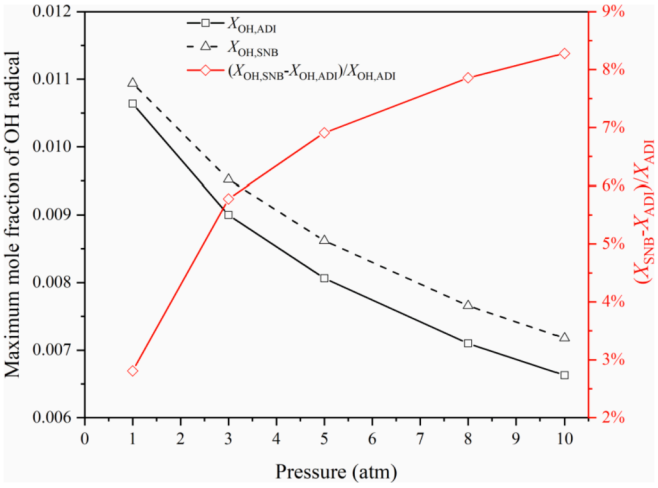

Fig. 12. Maximum mole fraction of OH radicals at various pressures for RP-3/$H_2O/O_2/N_2$ mixtures (ϕ = 1.0, T_{in} = 420 K, $H_2O/O_2/N_2$ = 12%/21%/67%).

$H_2O + M$ was the most influential one. However, the influence on flame speed of the important generation pathway of H radicals, HCO + M = H + CO + M, continually waned as pressure increased. The major formation pathway of OH radicals, $HO_2 + H = 2OH$ appeared among the most sensitive reactions for flame speed at various pressures. This indicated OH radicals became relatively more important to laminar flame speed at various pressure conditions. This agrees with our previous observation [21,25,26] that OH radicals were also strongly correlated with laminar flame speed. The relative difference of maximum mole fraction of OH radicals shown in Fig. 12 increased from 2.81% to 8.28% when pressures varied from 1 to 10 atm, which was consistent with the variation trend of relative difference for laminar flame speed in Fig. 9.

Sensitivity analysis and ROP analysis were performed for OH radicals at various pressures for RP-3/$H_2O/O_2/N_2$ mixtures as shown in Fig. 13. It indicated that the ROP values for all reactions increased with pressure. The reactions H + OH + M = H_2O + M and CO + OH = CO_2 + H consumed the most OH radicals and reactions $O + H_2O = 2OH$ and $H + O_2 = O + OH$ were the main paths for OH generation. Also considering the sensitivity analysis, the temperature-sensitive chain branching reaction [20,27], so as to more susceptible to radiation reabsorption, $H + O_2 = O + OH$ was the dominant reaction in the determine of the concentration of OH radicals (Fig. 14.).

Fig. 13 shows the effects of inlet temperature on ROP values for reaction $H + O_2 = O + OH$ at various pressures. It is evident that the generation of OH radicals by this reaction was inhibited by the elevated inlet temperature, although only less than 1% in the investigated pressure range. Moreover, this inhibition was slightly relieved at increasing pressures, resulting in the increasing relative difference of peak OH mole fraction in Fig. 12. Besides, the reaction $H + O_2 = O + OH$ facilitated the laminar flame speed according to the sensitivity analysis in Fig. 11, while its inhibition by radiation reabsorption induced preheat depressed its ability to promote flame speed. The weak inhibition on reaction $H + O_2 = O + OH$ at rising pressures led to the rising relative differences on laminar flame speeds at P = 1–10 atm as shown in Fig. 9.

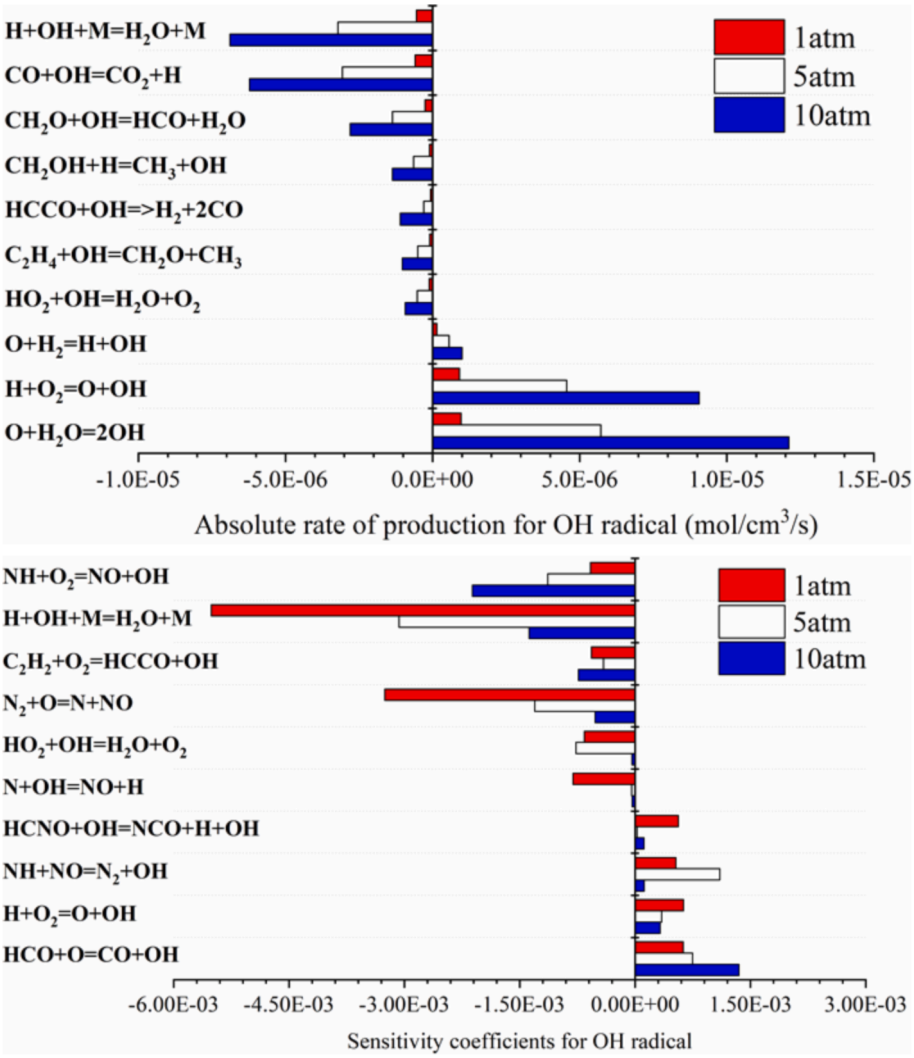

Fig. 13. ROP (a) and sensitivity (b) analyses for OH radicals at three pressures for RP-3/$H_2O/O_2/N_2$ mixtures ($\phi = 1.0$, $T_{in} = 420$ K, $H_2O/O_2/N_2 = 12\%/21\%/67\%$).

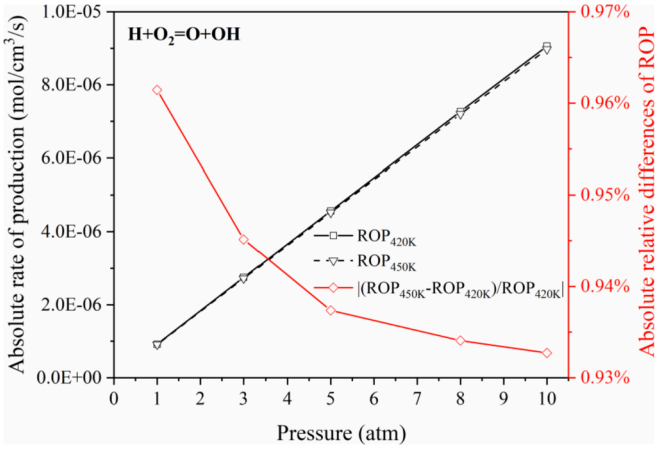

Fig. 14. ROP values for reaction H + O_2 = O + OH with two different inlet temperatures for RP-3/$H_2O/O_2/N_2$ mixtures ($\phi = 1.0$, $T_{in} = 420$ K and 450 K, $H_2O/O_2/N_2 = 12\%/21\%/67\%$).

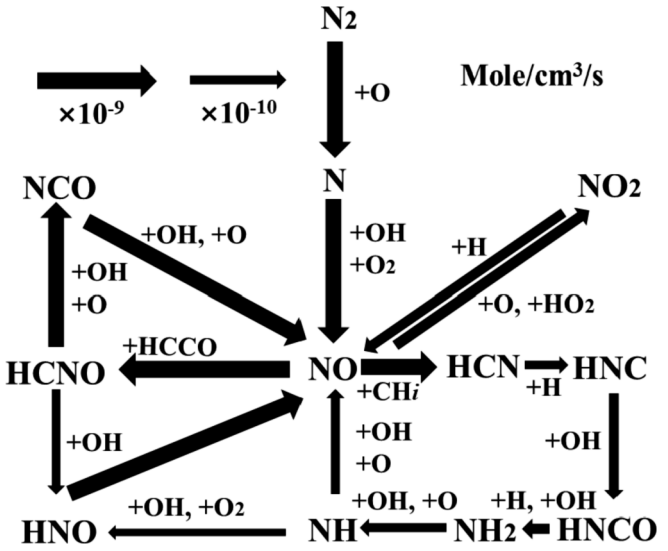

Fig. 15. Reaction pathway of NO during RP-3/$H_2O/O_2/N_2$ combustion ($\phi = 1.0$, $P = 1$ atm, $T_{in} = 420$ K, $H_2O/O_2/N_2 = 12\%/21\%/67\%$). Reactions with rates less than 5×10^{-10} mol/cm^3/s are neglected.

3.2. Effects on NO emission

3.2.1. At various equivalence ratios

To investigate the mechanism of radiation reabsorption affecting NO

emission, the reaction pathway of NO is shown quantitatively in Fig. 15. Because the fuels did not contain any N element, the initial production of NO only originated from N_2 in the air through the extended Zeldovich mechanism, which is an important NO formation pathway in the combustion of nitrogen-free fuels in air. The rate-limiting reaction was $N_2 + O = N + NO$, where the break of covalent N-N bond was greatly affected by temperature. Thus, it is straightforward to assume the thermal effect of radiation reabsorption on NO emission was mainly through the lowered temperature caused by radiative heat loss, which in turn reduced NO formation. Meanwhile, NO was consumed via the reactions with CH_i (the NO reburning mechanism [28]) and HCCO (rapid reduction of NO*x* [29]). Subsequently, after through intermediates such as HCN, HNCO and NH_i, N element was partially converted back to NO, with the participation of H, OH and O radicals [30]. Therefore, the other mechanism of radiation reabsorption effect on NO emission, namely the chemical effect, promoted NO formation via the increased radical concentrations (see Fig. 2).

The outlet mole fractions of NO calculated by ADI and SNB are depicted in Fig. 16. NO emission was significantly lower when radiation reabsorption was considered in the simulations. The discrepancy (relative difference between ADI and SNB results) first increased to a peak value of 61.47% at ϕ = 0.70–0.75, then decreased within equivalence ratios ϕ = 0.75–1.00. The same trend occurred again under the rich-fuel conditions, with a turning point of ϕ = 1.15 and a minimum value of 8.05% at ϕ = 1.40.

To discuss the radiation effect on NO emission during RP-3/H_2O/O_2/N_2 combustion, the detailed mechanisms of radiation-induced chemical effect and thermal effect on NO emission are illustrated next. As mentioned above, the thermal effect induced by radiation reabsorption was reflected by the relative difference of temperature in the post-flame zone between the ADI and SNB, as shown in Fig. 17. The SNB-obtained temperatures were generally lower than those of ADI due to the radiation heat transfer to the colder upstream. The relative difference of temperature decreased from 12.49% at ϕ = 0.7 to 4.84% at ϕ = 1.0, and then increased to 7.52% at ϕ = 1.4. Accordingly, the reduction on NO formation by this thermal effect first decreased and then increased. Obviously, this was not in accordance with the trend of relative difference for NO emission in Fig. 16 at ϕ = 0.70–0.75 and 1.15–1.40, which hence should be a result of the chemical effect as further discussed below.

Since the chemical effect is generally embodied by key radicals, the maximum mole fractions of radicals associated with NO reaction (H, OH and O, as shown in Fig. 15) calculated by ADI and SNB are shown in Fig. 18. It indicates that OH radicals were abundant in the fuel-lean

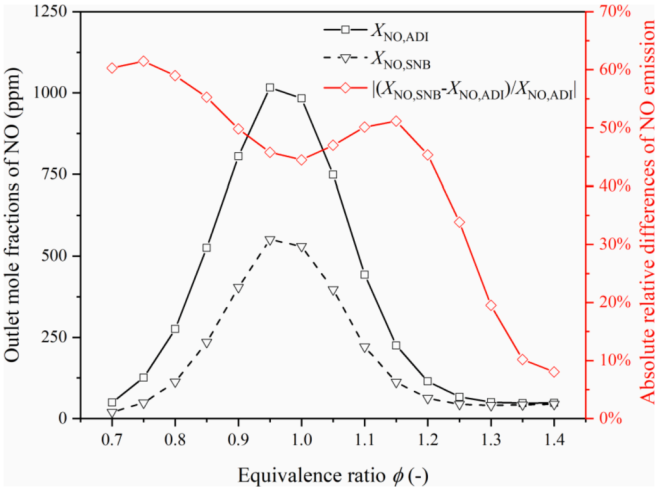

Fig. 16. Outlet mole fractions of NO at various equivalence ratios for RP-3/H_2O/O_2/N_2 mixtures (P = 1 atm, T_{in} = 420 K, H_2O/O_2/N_2 = 12%/21%/67%).

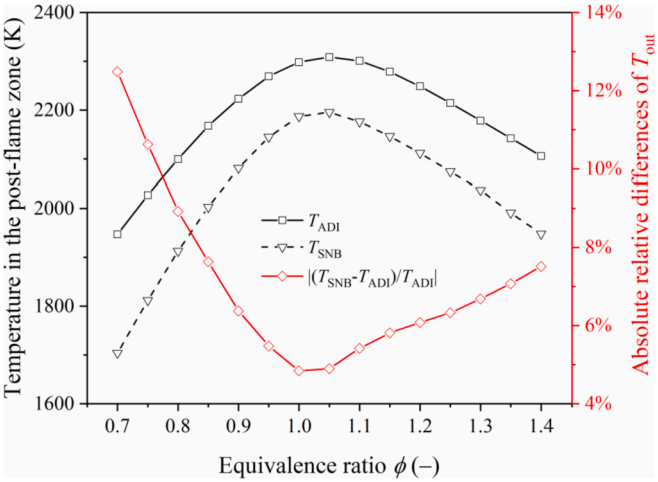

Fig. 17. Outlet temperatures calculated by ADI and SNB at various equivalence ratios for RP-3/H_2O/O_2/N_2 mixtures (P = 1 atm, T_{in} = 420 K, H_2O/O_2/N_2 = 12%/21%/67%).

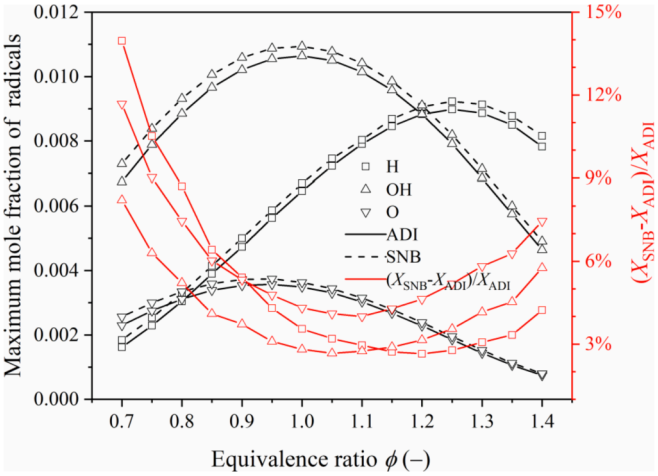

Fig. 18. Peak concentrations of radicals at various equivalence ratios for RP-3/H_2O/O_2/N_2 mixtures (P = 1 atm, T_{in} = 420 K, H_2O/O_2/N_2 = 12%/21%/67%).

mixtures and the concentration of H radicals was highest in the fuel-rich mixtures, while the mole fraction of O radicals was relatively low in the whole equivalent ratio range. After considering radiation reabsorption, all peak concentrations of radicals via SNB were higher than those via ADI. The variation of H radicals was more significant in fuel-lean mixtures while that of O radicals dominated in fuel-rich mixtures. It is worth noting that all the relative differences of radicals were greater in lean and rich conditions, which could possibly explain the nonlinear radiation reabsorption effects (ϕ = 0.70–0.75 and 1.15–1.40) on NO emission in Fig. 16.

As shown in Fig. 18, the increments of radical peak concentrations existed throughout the investigated equivalence ratios, indicating that chemical effect promoted NO emission for kerosene flames, i.e., reduced the SNB-ADI relative differences in Fig. 16. As equivalence ratio varied from 0.70 to 0.75, the relative differences of peak concentrations (shown in Fig. 18) decreased for all radicals, indicating the chemical effect promoting NO formation decreased. Thus, the relative differences of NO emission increased at ϕ = 0.70–0.75. At ϕ = 0.75–1.15, the increment of radical concentration was trivial and chemical effect was not significant. The relative difference of NO emission decreased under the control of thermal effect and the same variation trend can be observed within this range (shown in Figs. 15 and 16, respectively). Subsequently, the

increased chemical effect on NO formation resulted in the decrement of relative difference of NO emission at the range of $\phi > 1.15$.

3.2.2. At various pressures

Similarly, the NO emissions calculated by ADI and SNB for RP-3/$H_2O/O_2/N_2$ mixtures at different pressures are shown in Fig. 19. It indicates that the outlet mole fractions of NO first increased then decreased with rising pressures. This behavior was due to the increasing temperature and decreasing concentrations of radicals as shown in Fig. 20 and Fig. 21, respectively. The peak value of NO emission obtained by ADI was 2248.90 ppm at $P = 5$ atm and it was 1856.93 ppm at $P = 10$ atm by SNB, with the relative differences due to radiation reabsorption effect decreased from 44.48% to 16.84% as pressure increased from 1 to 15 atm.

Likewise, the thermal effect and chemical effect on the decreasing relative difference of NO emission with rising pressures were clarified. On the one hand, the thermal effect on NO emission, as indicated by the relative difference of temperatures shown in Fig. 20, decreased monotonically, which caused the relative difference of NO emission decreased with increasing pressures. On the other hand, the relative differences of H, OH and O radicals all increased with increasing pressures. It is thus manifested that the chemical effect of radiation reabsorption on NO formation was strengthened at higher pressures, which would reduce the relative difference of NO emission between the two radiation models. Consequently, the combination of the chemical and thermal effects resulted in the continuous attenuation of the relative difference for NO emission at $P = 1$–15 atm shown in Fig. 19.

4. Conclusions

In this article, the radiation reabsorption effects on laminar flame speed and NO emission during RP-3/$H_2O/O_2/N_2$ combustion was numerically evaluated as a function of equivalence ratio and pressure (in the range of $\phi = 0.7$–1.4 and $P = 1$–15 atm). On the one hand, mechanisms affecting the laminar flame speed due to two aspects of radiation reabsorption, namely direct radiative effect and preheat-induced chemical effect, were revealed and quantified. On the other hand, the roles of these two factors on NO emission were determined. The main conclusions of this work are as follow:

1. The radiation reabsorption of water vapor in vitiated air introduced by hydrogen heater had significant influence on the accurate simulation of laminar flame speeds. Along with rising equivalence ratios, the relative difference on laminar flame speeds between SNB- and ADI-results at atmospheric pressure first decreased and then increased, with the maximum value ($(S_{L,SNB}-S_{L,ADI})/S_{L,ADI} = 12.60\%$) occurred under a fuel-lean condition (at $\phi = 0.7$). The reaction $CH_2OH + H = CH_3 + OH$ played an important role in promoting laminar flame speeds when radiation reabsorption was considered. The chemical inhibition on the reversed step of $CH_2OH + H = CH_3 + OH$ first increased and then decreased, resulting in an opposite variation trend of laminar flame speeds.
2. As pressure was elevated, the radiation reabsorption effects on laminar flame speeds aggravated, by up to 12.41% at $P = 15$ atm. Chemical effects dominated at pressures 1–10 atm. The chain branching reaction related to OH radicals, which is more susceptible to radiation reabsorption, $H + O_2 = O + OH$ was the dominant reaction, and its promotion effect on the laminar flame speeds due to radiation reabsorption increased at higher pressures. Above 10 atm, the increment of absorption coefficient with pressure was greater than that of optical thickness, resulting in a slight increase in the SNB-ADI relative difference of laminar flame speeds at 10–15 atm by direct radiative effect.
3. For NO emission during RP-3/$H_2O/O_2/N_2$ combustion, flame temperature and radical concentrations were two important factors determining NO emission. The reduction of downstream temperature

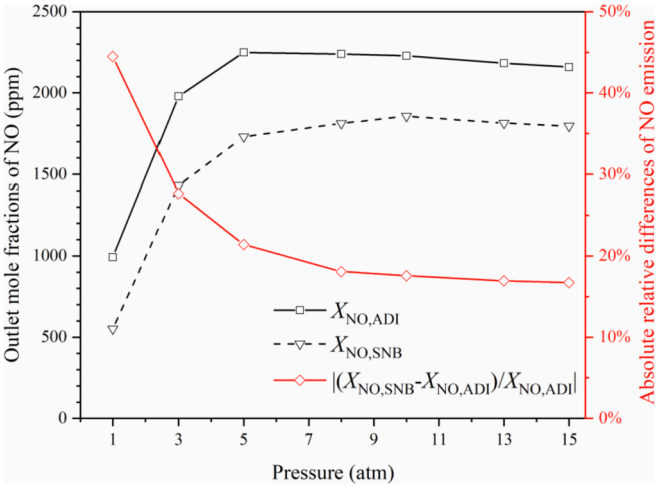

Fig. 19. Outlet mole fractions of NO at various pressures for RP-3/$H_2O/O_2/N_2$ mixtures ($\phi = 1.0$, $T_{in} = 420$ K, $H_2O/O_2/N_2 = 12\%/21\%/67\%$).

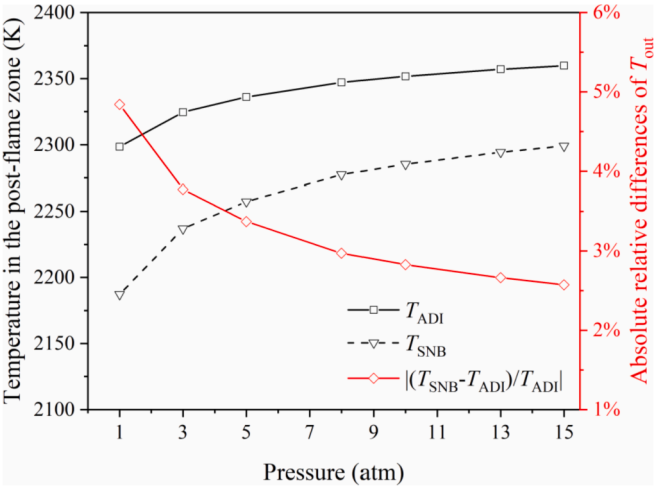

Fig. 20. Outlet temperatures calculated by ADI and SNB at various pressures for RP-3/$H_2O/O_2/N_2$ mixtures ($\phi = 1.0$, $T_{in} = 420$ K, $H_2O/O_2/N_2 = 12\%/21\%/67\%$).

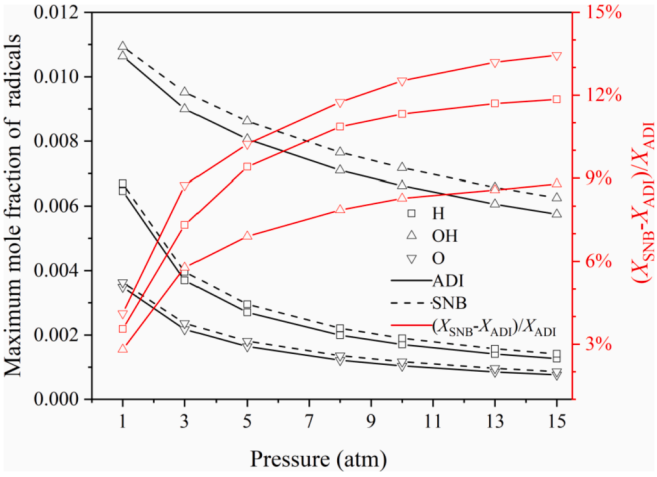

Fig. 21. Maximum mole fractions of radicals at various pressures for RP-3/$H_2O/O_2/N_2$ mixtures ($\phi = 1.0$, $T_{in} = 420$ K, $H_2O/O_2/N_2 = 12\%/21\%/67\%$).

caused by radiative heat loss and the increment of radical concentrations due to radiation-induced-preheat in the inlet were the controlling factors of radiation reabsorption effects on NO emission. As equivalence ratios varied, the competition between chemical effect and thermal effect led to the non-monotonic trend of relative difference for NO emission, with a peak value of 61.47% at $\phi = 0.75$. With rising pressures, the consistent decrease of thermal effect and increase of chemical effect made the contribution of radiation on NO emission most pronounced at $P = 15$ atm.

CRediT authorship contribution statement

Shu Zheng: Methodology, Formal analysis, Investigation, Conceptualization, Writing – original draft. **Hao Liu:** Writing – review & editing, Data curation, Methodology. **Qing Li:** Writing – review & editing, Software. **Jiajian Zhu:** Validation. **Mingbo Sun:** Supervision. **Bo Zhou:** Formal analysis. **Ran Sui:** Writing – review & editing. **Qiang Lu:** Supervision, Project administration.

Declaration of Competing Interest

The authors declare that they have no known competing financial interests or personal relationships that could have appeared to influence the work reported in this paper.

Acknowledgements

This work was supported by the National Natural Science Foundation of China (No. 51976057 and 51922040), the Science and Technology Innovation Program of Hunan Province (2020RC5008) and the Fundamental Research Funds for the Central Universities (No. 2020JG005, 2020DF01).

Appendix A. Supplementary data

Supplementary data to this article can be found online at https://doi.org/10.1016/j.fuel.2022.124545.

References

[1] Das N, Pandey KM, Sharma KK. A brief review on the recent advancement in the field of jet engine - scramjet engine. Mater Today: Proc 2021;45:6857–63.
[2] Tian Y, Zeng X, Yang S, Zhong F, Le J. Study on the effects of thermal throat on flame stabilization in a kerosene fueled supersonic combustor. Energy Convers Manage 2018;166:98–105.
[3] Ma H, Xie M, Zeng W, Chen B. Experimental study on combustion characteristics of Chinese RP-3 kerosene. Chin J Aeronaut 2016;29:375–85.
[4] Ingenito A. NO_x reduction strategies in scramjet combustors. Aerosp Sci Technol 2016;59:189–98.
[5] Evans MJ, Chinnici A. Water vapour effects on temperature and soot loading in ethylene flames in hot and vitiated coflows. Proc Combust Inst 2021;38:5383–91.
[6] Sun W, Huang W, Qin X, Deng Y, Kang Y, Peng W, et al. Water impact on the autoignition of kerosene/air mixtures under combustor relevant conditions. Fuel 2020;267.
[7] Shi W, Tian Y, Zhang W-Z, Deng W-X, Zhong F-Y, Le J-L. Experimental investigation on flame stabilization of a kerosene-fueled scramjet combustor with pilot hydrogen. J Zhejiang Univ-Sci A 2020;21:663–72.
[8] Chang L, Lin Y, Cao Z, Xu L. Effects of water vapor addition on NO reduction of n-decane/air flames. Energy Sources Part A 2019;42:1526–40.
[9] Ju Y, Masuya G, Ronney PD. Effects of radiative emission and absorption on the propagation and extinction of premixed gas flames. Symp (Int) Combust 1998;27:2619–26.
[10] Yoshinaga K, Kobayashi H. Numerical Study of Radiation Effects on Polypropylene Combustion Using High-temperature Oxidizer Diluted with H_2O and CO_2. J Therm Sci Technol 2008;3:167–78.
[11] Sohn CH, Chen Z, Ju Y. Effects of radiation on the uncertainty of flame speed determination using spherically propagating flames with $CO/CO_2/H_2O$ dilutions at elevated pressures. Int J Heat Mass Transf 2015;86:820–5.
[12] Wang J, Niioka T. Numerical study of radiation reabsorption effect on NOxformation in CH_4/air counterflow premixed flames. Proc Combust Inst 2002;29:2211–7.
[13] Yan Y, Liu Y, Fang W, Liu Y, Li J. A simplified chemical reaction mechanism for two-component RP-3 kerosene surrogate fuel and its verification. Fuel 2018;227:127–34.
[14] Ma H, Fu S, Wu Z, Liu Y, Zeng W. Review of combustion characteristics and reaction mechanism construction of RP-3 aviation kerosene. Aeroengine 2021;47:25–31.
[15] Liu X, Wang Y, Bai Y, Zhou Q, Yang W. Development and verification of a physical–chemical surrogate model of RP-3 kerosene with skeletal mechanism for aircraft SI engine. Fuel 2022;311.
[16] Kee RJ, Grcar JF, Smooke MD, Miller JA, Meeks E. PREMIX: A FORTRAN Program for Modeling Steady Laminar One-Dimensional Premixed Flames; 1985.
[17] Lamoureux N, Merhubi HE, Pillier L, de Persis S, Desgroux P. Modeling of NO formation in low pressure premixed flames. Combust Flame 2016;163:557–75.
[18] Zheng S, Sui R, Yang Y, Sun Y, Zhou H, Lu Q. An improved full-spectrum correlated-k-distribution model for non-gray radiative heat transfer in combustion gas mixtures. In: International Communications in Heat and Mass Transfer; 2020. p. 114.
[19] Zheng S, Sui R, Liang W, Zhou H, Law CK. On band lumping, radiation reabsorption, and high-pressure effects in laminar flame propagation. Combust Flame 2020;221:86–93.
[20] Zheng S, Liu H, Sui R, Zhou B, Lu Q. Effects of radiation reabsorption on laminar NH_3/H_2/air flames. Combust Flame 2022;235.
[21] Zheng S, Liu H, Li D, Liu Z, Zhou Bo, Lu Q. Effects of radiation reabsorption on the laminar burning velocity of methane/air and methane/hydrogen/air flames at elevated pressures. Fuel 2022;311:122586.
[22] Zheng S, Yang Y, Sui R, Lu Q. Effects of C_2H_2 and C_2H_4 radiation on soot formation in ethylene/air diffusion flames. Appl Therm Eng 2021;183.
[23] Zhang A-Y, Wang F-Q, Cheng Z-M, Liang H-X, Shi X-H. Radiative property investigation of dispersed particulate medium with the consideration of non-uniform particle size distribution and dependent scattering effects. Int J Coal Sci Technol 2022;186:122488.
[24] Tian Y, Yang S, Le J, Zhong F, Tian X. Investigation of combustion process of a kerosene fueled combustor with air throttling. Combust Flame 2017;179:74–85.
[25] Zheng S, Shi Y-X, Wang Z-Q, Wang P-J, Liu G, Zhou H-C. Development of new technology for coal gasification purification and research on the formation mechanism of pollutants. Int J Coal Sci Technol 2021;8:335–48.
[26] Okafor EC, Naito Y, Colson S, Ichikawa A, Kudo T, Hayakawa A, et al. Experimental and numerical study of the laminar burning velocity of CH_4–NH_3–air premixed flames. Combust Flame 2018;187:185–98.
[27] Hu E, Huang Z, He J, Miao H. Experimental and numerical study on lean premixed methane–hydrogen–air flames at elevated pressures and temperatures. Int J Hydrogen Energy 2009;34:6951–60.
[28] Berg PA, Smith GP, Jeffries JB, Crosley DR. Nitric oxide formation and reburn in low-pressure methane flames. Symp (Int) Combust 1998;27:1377–84.
[29] Perry RA, Siebers DL. Rapid reduction of nitrogen oxides in exhaust gas streams. Nature 1986;324:657–8.
[30] Liu J, Zhao W, Fan X-R, Xu M-X, Zheng S, Lu Q. Effect of alkali metal ions on the formation mechanism of HCN during pyridine pyrolysis. Int J Coal Sci Technol 2021;8:349–59.